



## OPEN ACCESS

## EDITED BY

Yuan-Pin Chang,  
National Sun Yat-sen University, Taiwan

## REVIEWED BY

Amir Ismail,  
Texas A&M University Corpus Christi,  
United States  
Chieh-Wei Hsu,  
National Kaohsiung University of Science and  
Technology, Taiwan

## \*CORRESPONDENCE

Shilin Wang,  
✉ ybybws1@163.com  
Ahmed Mansour,  
✉ ahmedmans48@amu.edu.eg

RECEIVED 08 February 2025

ACCEPTED 03 June 2025

PUBLISHED 27 June 2025

## CITATION

Wang S, Guo X, Su P, Li L, Ahmed MS, Chu X,  
Zhang X, Gentzis T and Mansour A (2025)  
Sources of shallow natural gases in the  
Longgang marine gas field, NE Sichuan Basin:  
an example from the water conveyance  
tunnel.  
*Front. Earth Sci.* 13:1573369.  
doi: 10.3389/feart.2025.1573369

## COPYRIGHT

© 2025 Wang, Guo, Su, Li, Ahmed, Chu,  
Zhang, Gentzis and Mansour. This is an  
open-access article distributed under the  
terms of the [Creative Commons Attribution  
License \(CC BY\)](https://creativecommons.org/licenses/by/4.0/). The use, distribution or  
reproduction in other forums is permitted,  
provided the original author(s) and the  
copyright owner(s) are credited and that the  
original publication in this journal is cited, in  
accordance with accepted academic practice.  
No use, distribution or reproduction is  
permitted which does not comply with  
these terms.

# Sources of shallow natural gases in the Longgang marine gas field, NE Sichuan Basin: an example from the water conveyance tunnel

Shilin Wang<sup>1\*</sup>, Xiangqian Guo<sup>1</sup>, Peidong Su<sup>1</sup>, Long Li<sup>2</sup>,  
Mohamed S. Ahmed<sup>3</sup>, Xiaojin Chu<sup>4</sup>, Xiangbing Zhang<sup>4</sup>,  
Thomas Gentzis<sup>5</sup> and Ahmed Mansour<sup>1,6\*</sup>

<sup>1</sup>School of Geoscience and Technology, Southwest Petroleum University, Chengdu, China, <sup>2</sup>Sichuan Water Development Investigation, Design & Research Co., Ltd, Chengdu, China, <sup>3</sup>Department of Geology and Geophysics, College of Science, King Saud University, Riyadh, Saudi Arabia, <sup>4</sup>China Railway 18th Bureau Group Corporation, Ltd., Tianjin, China, <sup>5</sup>Core Laboratories LP, Houston, TX, United States, <sup>6</sup>Geology Department, Faculty of Science, Minia University, Minia, Egypt

With the advancement of the Tingzikou Irrigation Area Water Diversion Project, the issue of harmful shallow underground gases in the tunnel has become increasingly prominent. Identifying the causes, sources, and migration processes of these harmful gases is crucial to prevent possible catastrophic impacts and mitigation during tunnel construction. Here, we apply an integrated approach of carbon isotope composition to analyze the geochemical characteristics of shallow natural gas components from a high-gas water diversion tunnel in the Tingzikou Irrigati Area. Results are integrated and compared with data from the Sichuan Basin fault system and isotopic values from different strata to provide further evidence of the source of shallow natural gas in the area. The geochemical characteristics of the gas samples reveal that the methane content is the most abundant, and constitutes as high as 45.16%, while carbon oxides are in the range of 0.02%–0.1%. Heavier hydrocarbons (C<sub>2</sub>+ ) account for 2.27%, and the dryness coefficient is 0.96. These major components indicate the presence of wet gas with relatively low thermal maturity. The alkane gases exhibit a normal carbon sequence, with  $\delta^{13}\text{C}_1$  values less than  $-25\text{‰}$ , indicating that the gas originates from oil-type organic. The carbon dioxide is classified as Type II inorganic gas, and the hydrogen sulfide is attributed to thermochemical sulfate reduction origin. In the tunnel area,  $\delta^{13}\text{C}_2$  ranges from  $-29.53\text{‰}$  to  $-28.11\text{‰}$ , with an average of  $-28.80\text{‰}$ , which are similar to the ethane isotope values of the J<sub>1</sub>l and J<sub>1</sub>m strata in the central Sichuan Basin, but heavier than those of the J<sub>1</sub>dn, J<sub>1</sub>d, and T<sub>2</sub>l strata, and significantly different from T<sub>3</sub>x. This reveals that the shallow natural gas originates from the shallow oil and gas source rock layers of the Ziliujing Formation at the Ziliujing anticline, making it a “self-generated and self-stored” gas.

## KEYWORDS

carbon isotopes, harmful gases, Sichuan Basin, shallow gas characteristics, water diversion tunnel

# 1 Introduction

The Tingzikou Irrigation project is a large-scale water conservancy project for irrigation and urban-rural water supply, serving 13 counties across four cities: Guangyuan, Nanchong, Guang'an, and Dazhou. The main canal traverses a weak red-layer zone that is coal-free, with six anticline gas-bearing structures distributed along the route. Several tunnels are located in the Yuanba and Longgang oil and gas areas (Figure 1), where multiple combustion incidents have occurred during construction.

As construction activities progress, the development and utilization of underground space have become increasingly necessary. However, the construction of tunnels in complex environments rich in hazardous gases frequently results in accidents of gas hazardous include the following examples: in 1971, a gas explosion in an 8.85 km long hard-rock hydraulic tunnel passing in Los Angeles, United States, resulted in 17 fatalities (Richard, 2002). In 1984, methane gas leaked from a fracture at the end of the Lancashire water tunnel in England, causing an explosion that killed 16 and injured 28 members of a visiting group (Pearson et al., 1992). In 2007, high concentrations of hydrogen sulfide and methane were detected in Zagros tunnel in Iran, led to a 4-month work stoppage (Shahriar et al., 2009). Furthermore, records of hazardous gas accidents were reported from various types of tunnels in Turkey (Copur et al., 2012) and Taiwan (Sortino et al., 2022). Other gas explosions with varying degrees of casualties have occurred in tunnels like the Baitaishan tunnel on the

Dacheng Railway, Dongjiashan tunnel on the Du-Wen Highway, Qishanyan tunnel on the Cheng-Gui Railway, and Xingapo tunnel on the Xubi Railway (Ding et al., 2018). These catastrophic events underscore the urgent need to address the hazards of harmful gases like methane in tunnel construction.

The types and characteristics of hazardous gases in tunnels are closely related to the surrounding geological environment. Previous studies have extensively studied the composition, migration, and accumulation characteristics of shallow hazardous gas in non-coal formations (Chen et al., 2019), the analysis of harmful gas composition and enrichment locations in the Kangding section of the Sichuan-Tibet line (Chen et al., 2019), the complex structural zone of western Sichuan (Yuan et al., 2023), and related processes of migration and diffusion of inorganic carbon monoxide and hydrogen sulfide from deep mantle through fault zones and granite alteration belts (Su et al., 2020; Sabrekov et al., 2023).

Although several studies have focused on gas hazardous, primarily in the context of shallow oil and gas exploration (Tan et al., 2022) and non-coal railway and highway engineering (Su et al., 2021), the formation and migration patterns of shallow natural gas in hydraulic tunnels in central Sichuan have not been systematically studied. The shallow natural gas escape of hydraulic tunnel has the characteristics of special construction technology, shallow buried depth of tunnel and strong randomness of shallow natural gas distribution. At present, the causes, sources, transportation and storage of gas mainly focus on energy fields such as oil and coal

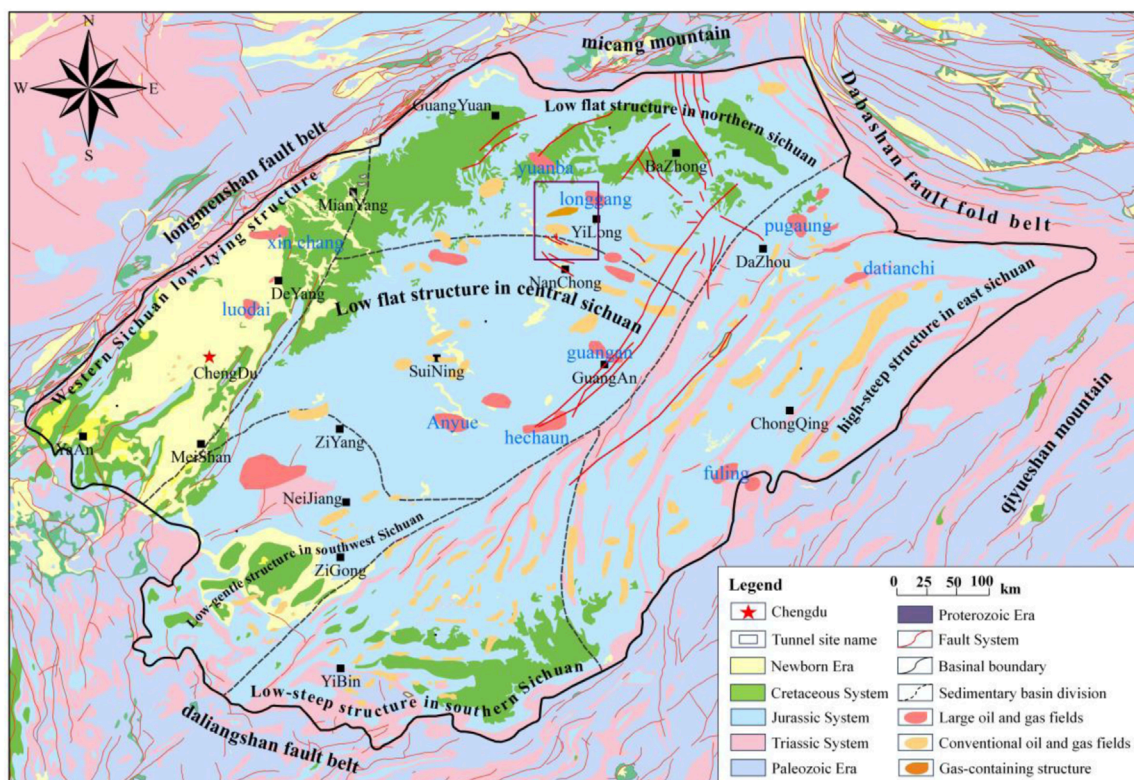


FIGURE 1 Structural map of the study area. Showing the location of the studied tunnel area in the hilly terrain of the central Sichuan Basin (Zhang et al., 2022; Liu et al., 2024; Bai et al., 2024) This area is characterized by the gently undulating structure from the central to northern Sichuan.

mines. In the field of hydraulic tunnel construction, there is a lack of effective parameters for identifying different sources of shallow natural gas, and a comprehensive identification chart for identifying the causes and sources of shallow natural gas has not been established. This paper can not only provide a theoretical basis for the resource evaluation and accumulation mechanism of shallow natural gas, but also provide theoretical guidance for the prediction of shallow natural gas reservoirs. Based on field work sampling of harmful gases during tunnel drilling in the Tingzikou Irrigation area and laboratory test results of gas composition, the aims of this study are to: (1) identify the types and sources of harmful gases encountered in the studied area; and (2) reveal the mechanisms of shallow natural gas on a comprehensive geological investigation and their relationship to regional structures.

## 2 Geologic settings

The tunnel is located in the northeastern part of the Sichuan Basin in the Longgang marine gas field, within the northern Sichuan low and gentle belt (Figure 1). The tunnel area is structurally influenced by the northeast to southwest Jiulongshan Anticline Tectonic Belt, the south and southeast Cangxi-Bazhong Gentle Tectonic Belt, and the adjacent Tongnanba Anticline Tectonic Belt (Figure 1) (Renchun et al., 2019; Jiang, 2019), resulting in a fault system under compressive stress. To the east, it is bounded by the Huaying Mountains fault zone, while the Longquan Mountains fault zone lies to the west. Additionally, it is adjacent to the Longmenshan fault zone and the Micang-Daba fold belt to the northwest (Huang et al., 2023; Qian et al., 2023), situated in a region characterized by large-scale Mesozoic and Cenozoic oil and gas basins (Figure 1). This area is influenced by the surrounding fault zones, including the Huaying and Longquan Mountains, as depicted in Figure 1. The major structural features of the investigated tunnel in the Tingtougou Irrigation District include the Yilong, Shuanghechang, Yingshan and Tumengpu, as well as the Hongshanchang and Dashenshan synclines (Figures 1, 2). The Yilong Anticline is part of the Pingchang-Lianhua structural system, transitioning from a platform to the Shuanghechang Anticline. It extends 7 km with a saddle shape and symmetrical wings, a dip angle of 4°–6°, and an axis direction of 335° (Huang et al., 2023). In this region, the southeast end of the Jurassic base layer develops into a fold structure, with its plane position roughly overlapping the aforementioned anticlines.

The tunnel area passing across the Longgang large gas field in the western part of the Guangwang-Kaijiang-Liangping land shelf, east of the Puguang Gas Field (Figure 1). This gas field is characterized by a thick gas reservoir of reef buildups with a closure height of 42 m and a closure area of 5.7 km<sup>2</sup>. As of 2017, the proven reserves are 74.243 billion cubic meters, with a remaining recoverable volume of 39.244 billion cubic meters. The main producing layers include the Feixianguan Formation (T<sub>1</sub>f) and the Changxing Formation (P<sub>2</sub>ch) (Zhang et al., 2022; Liu et al., 2024; Bai et al., 2024). The Jurassic gas reservoirs primarily consist of hydrocarbons, with methane as the predominant component followed by a low sulfur content (Wang et al., 2023). The shallow natural gas in the Longgang gas field originates from multiple sets of Upper Triassic-Lower Jurassic source rocks. These include

mudstones of the Ziliujing Formation and the coal seams of the Xujiahe Formation (T<sub>3</sub>x).

The study area is characterized primarily by alternating layers of sandstone and mudstone, with gently dipping strata typical of red beds. At the tunnel entrance, the surface layer is composed of loose colluvial deposits (Q<sub>4</sub><sup>col+dl</sup>) consist of boulders and gravels. In contrast, the surface cover at the tunnel exit consists of residual slope deposits (Q<sub>4</sub><sup>dl+el</sup>) made up of clay. The surrounding rock within the tunnel belongs to the Middle Jurassic Suining Formation (J<sub>3</sub>s<sup>②</sup>), which is composed of silty mudstone interbedded with thin to medium-thick sandstone and muddy siltstone. The rock is weak, with strata orientations of N10°–30°W/SW and dip angles of 1°–4°. Faulting has significantly developed joints and fractures, resulting in fractured and soft geological conditions. During excavation process, minimal groundwater is encountered, but the tunnel remains susceptible to rockfalls and collapses, which poses significant safety risks and increases construction difficulties.

## 3 Material and methods

### 3.1 Study site

The high gas tunnel in the Tingtougou Irrigation District is located in Yilong County, Nanchong City, Sichuan Province. It covers a total length of 2,358 m, starting at the left side of the Guojiawan Gorge and terminating at the middle slope of Dengjia Liang Mountain (Zou et al., 2011). This tunnel is a critical component of the Tingtougou Irrigation District project. The ground elevation along the tunnel ranges from 411.5 m to 450.7 m, with an average slope of 15–22°. The maximum burial depth of the tunnel is 106.3 m. The surrounding rock at the tunnel face is primarily grade IV, exhibiting relatively poor stability and significant time dependent effects. The net internal cross-section measures 7.5–7.8 m and the design flow rate is 51.25 m<sup>3</sup>/sec. The tunnel is excavated using the drilling and blasting method (Sun et al., 2023) and the tunnel chamber follows the ridge line without deep-cut valleys.

### 3.2 On-site procedures using a sampling pump

The safety inspection personnel carried instruments to detect harmful gases, including methane, carbon monoxide, hydrogen sulfide, and carbon dioxide (Figures 5a–d), Instrument parameters are shown in Table 1.

They conducted continuous monitoring at three locations: the heading face, Borehole #1, and Borehole #2 (Figure 3). Monitoring points W1 through W6 were placed on the heading face, 3 cm from the tunnel perimeter, while borehole measurements were taken 2 cm from the borehole mouth.

The concentration readings were obtained as stable average values from 1 to 3 measurements, resulting in a total of 32 data sets. Using the “pre-vacuum sampling method” and the “water displacement gas collection method,” parallel samples were collected in gas-tight, leak-proof sample bags and bottles (Figure 4). These samples were taken from horizontal boreholes inside the

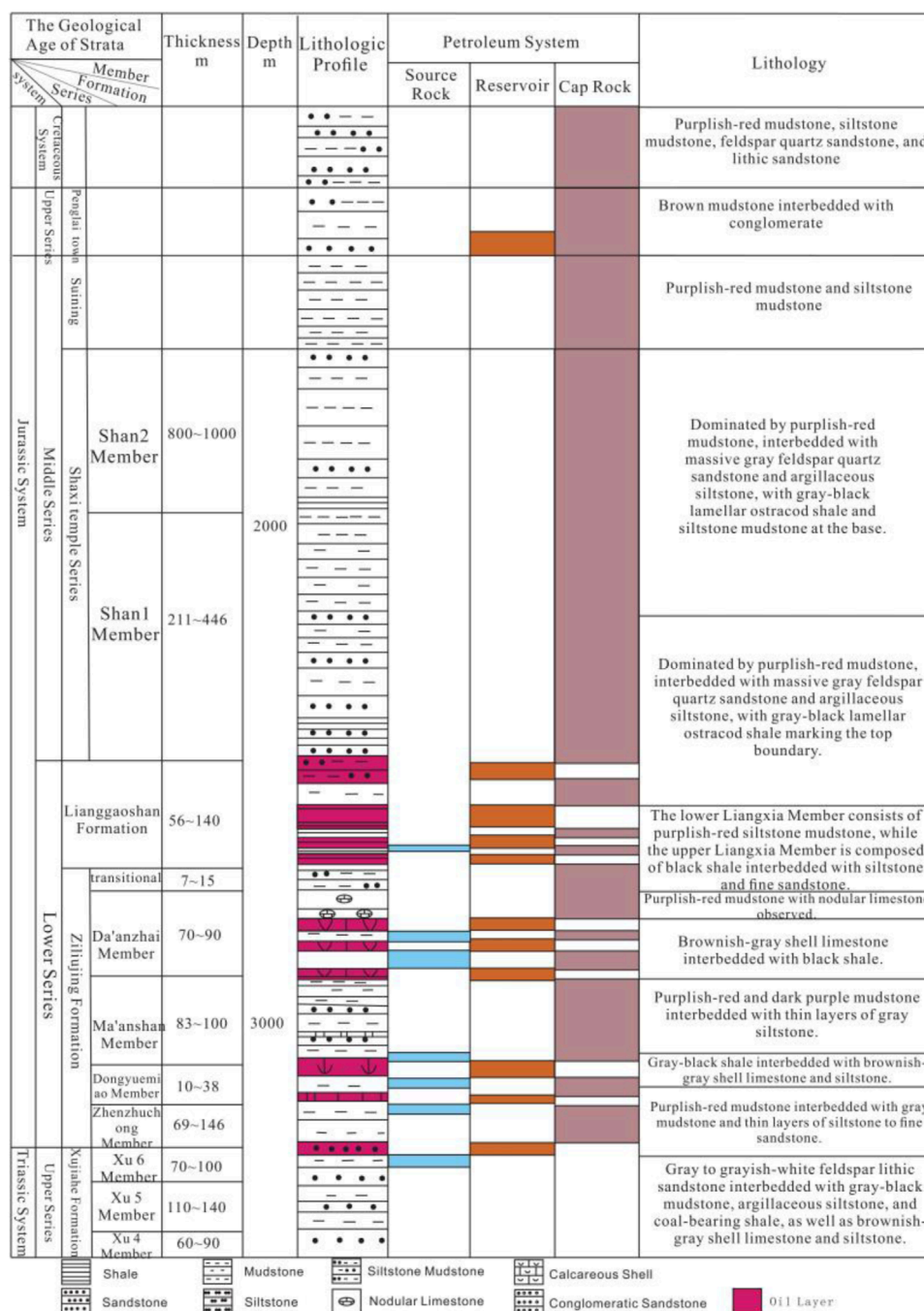


FIGURE 2 Stratigraphic Column in the Study Area (modified after (Guo et al., 2004; Li et al., 2016)). The main exposed strata include the Jurassic Suining Formation and Shaximiao Formation, as well as a smaller portion of thick to very thick sandstone layers from the Penglaizhen Formation.

tunnel and from the gas escape point on the right side of the heading face (W6) (Figure 3). The sampling interval was set at 20 min, resulting in a total of 9 bagged samples (Figure 5a) and 6 bottled samples (Figure 5b).

The specific sampling procedure consists of three main steps (Su et al., 2020), open the left valve of the gas collection bag, connect it to the rubber tube on the outlet of the gas sampling

pump, and quickly evacuate the air inside the bag. Afterwards, move the rubber tube to the right valve of the gas pump, maintaining a sampling speed of 0.05 L/min, and place the inlet of the gas pump at the sampling location. Unscrew the right valve of the gas pump. When the gas sample fills approximately two-thirds of the collection bag's capacity, stop the sampling process and tighten the valve.

TABLE 1 On-site Inspection Equipment Statistics used for on-site gas collection sampling.

Instrument model	Test content	Measurement Range (%)	LEL (%)
SL-808A	Methane	0~0.1/1	0.0005
CJG100	Methane、Carbon Dioxide	0~100	0.2
CJG10	Methane、Hydrogen Sulfide	0~10	0.02
BH-90A	Hydrogen Sulfide	0~100	1
AS8700A	Carbon Monoxide	0~0.1	0.0001

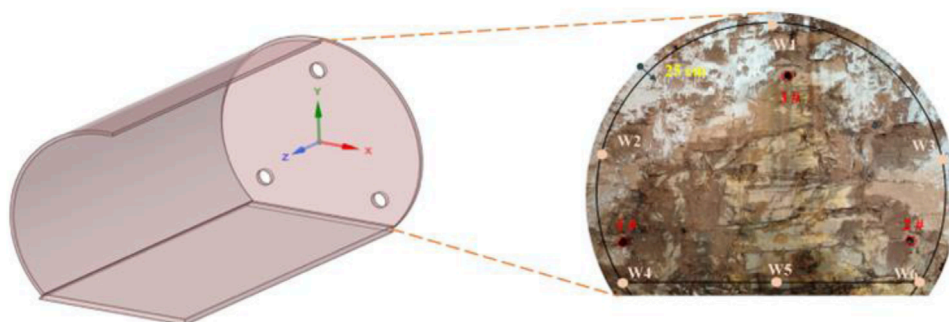


FIGURE 3 Schematic diagram of detection section point layout; where W1 to W2 are the measurement points for harmful gases, arranged for cross-sections., Points 1# to 3# represent horizontal drilling boreholes with a design hole depth of more than 50 m and a hole diameter of 75 cm.



FIGURE 4 Collect gas samples. (a) was used to obtain 5 groups of bagged samples by drainage and gas collection method, (b) was used to obtain 5 groups of bagged samples by drainage and gas collection method. B is the pre-vacuum sampling method to obtain 9 groups of bagged samples.

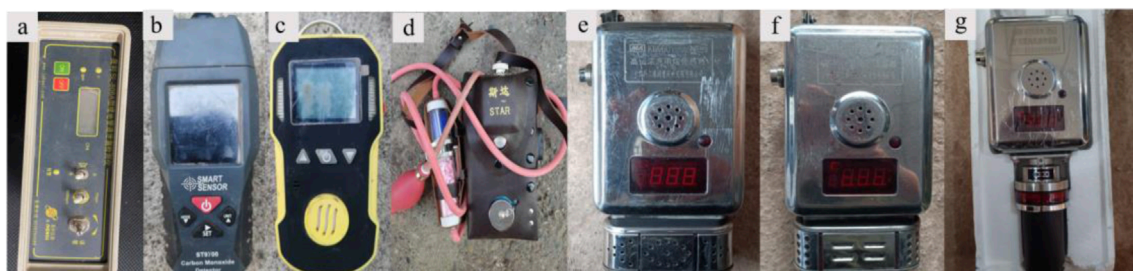
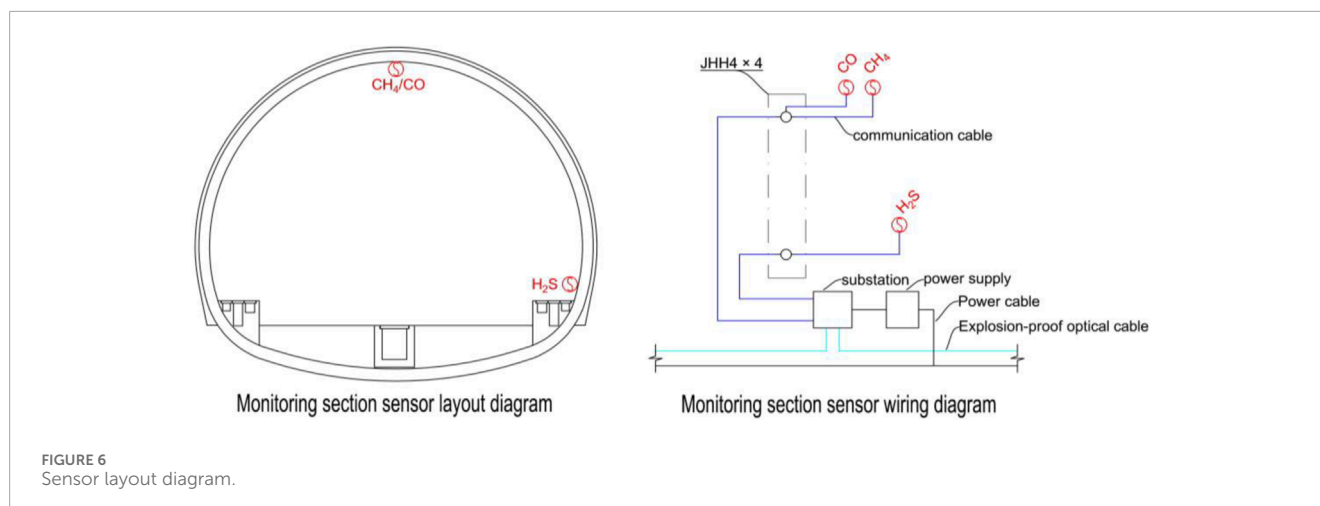


FIGURE 5 Detection and Digital Monitoring Sensors; (a) SL-808A Natural Gas Leak Detector; (b) AS8700A Carbon Monoxide Detector; (c) BH-90A Hydrogen Sulfide Detector; (d) CJG Optical Interference Combustible Gas Detector; (e-g) are Digital Monitoring equipment.



### 3.3 Gas collection procedure for drainage

The gas samples were collected in glass bottles using the water displacement method to ensure the airtightness of the sample bottles. The sampling technique is conducted based on inverting the glass bottle in water and open the stopper to fill the bottle completely with water. Then, one end of the rubber tube is placed at the gas emission point, whereas the other end is inserted into the glass bottle and the water level was monitored to control the volume of the collected gas. To ensure the purity of the collected gas, the mouth of the bottle is sealed and labeled when the water level inside the bottle reaches approximately 0.5–1 cm from the top. Overall, a total of five gas samples were collected using the water displacement method for stable carbon isotope analysis.

### 3.4 Digital Monitoring

To verify the authenticity and effectiveness of the on-site testing data, digital detection data of methane, carbon monoxide, and wind speed sensors were retrieved from the tunnel face between July 15 and 20. These sensors recorded continuous variations in wind speed. The methane and carbon monoxide sensors were positioned at the top of the tunnel face (Figures 5e,f), while the hydrogen sulfide sensor was located at the arch foot of the tunnel face (Figure 5g). Details of sensor arrangement Figure 6. Data were collected continuously with a sampling interval of 1 h. Each sensor was monitored independently for 100 h, resulting in a total of 4 sets of 400 real-time data points.

### 3.5 Gas chromatography-mass spectrometry (GC-MS)

A total of nine gas samples were analyzed using a SQL gas chromatography-mass spectrometry (GC-MS) system at the State Key Laboratory of Oil and Gas Reservoir Geology and Development Engineering, Southwest University of Petroleum (China). The gas samples (Figures 5e,f) were carefully transferred via a carrier gas through a separation capillary column (inner diameter 0.25 mm,

length 30 m) and separated in the GC-MS using a quadrupole with high-frequency voltage (Li et al., 2020). The temperature was raised to 200 °C, and each sample was ionized at an acceleration speed of 70 eV in the mass spectrometer, with a scanning interval of 0.1 s (Sortino et al., 2022; Maimaiti et al., 2022). Finally, the chemical components of the mixture were identified by interpreting spectra using a spectral library (Guo et al., 2004).

### 3.6 Stable carbon isotope ( $\delta^{13}\text{C}$ )

A total of five water samples were analyzed for carbon isotopes of organic compounds in harmful gases using an Isoprime100 isotope ratio mass spectrometer at the State Key Laboratory of Oil and Gas Reservoir Geology and Development Engineering, Southwest University of Petroleum. The measurements were conducted under a constant temperature of 25°C and a relative humidity of 70% (Guo et al., 2004). This analysis mainly includes the values of  $\delta^{13}\text{C}_1$ ,  $\delta^{13}\text{C}_2$ , and  $\delta^{13}\text{C}_3$ . Using an HP-PLOT/Q chromatographic column (inner diameter 30 × 0.25 mm, 0.25 μm 100% separating agent) (Araizaga et al., 2013; Talma and Esterhuyse, 2015), the natural gas in is separated to obtain pure gases (such as CH<sub>4</sub>, CO<sub>2</sub>, N<sub>2</sub>). The oven temperature was programmed at 40°C and held for 3 min, then ramped at a rate of 25°C/min to 160°C and maintained isothermally for 4 min. The analytical precision after duplication and sometimes triplication of  $\delta^{13}\text{C}$  analysis is typically better than ±0.3‰–0.5‰ (Talma and Esterhuyse, 2015; Adsul et al., 2023). The isotope reference material SY/T 7359-2017 was used following the petroleum and natural gas industry standard of the People's Republic of China, and referenced against the VPDB (Vienna Pee Dee Belemnite) standard (Aharon et al., 2022).

## 4 Results and discussion

### 4.1 Gas component characteristics

#### 4.1.1 On-site detection

In 2023 (July 15, at 16:30), active drilling at the heading face of a high-gas tunnel inlet in the Tingzikou Irrigation District

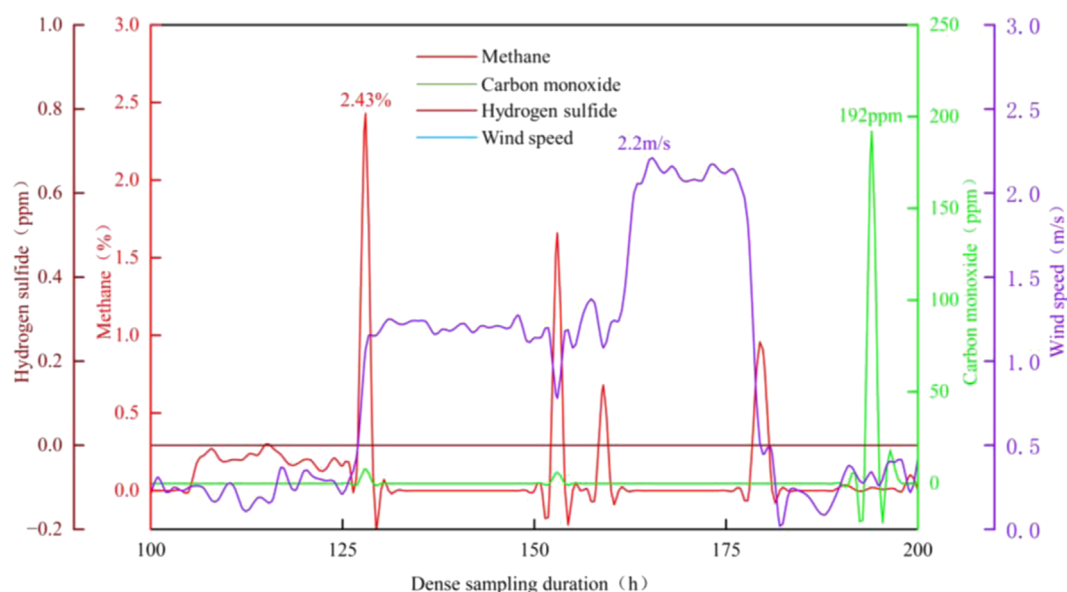


**FIGURE 7** Shows monitoring data from the digital platform, with the red line representing methane, the green line for carbon monoxide, the purple line for wind speed, and the maroon line representing hydrogen sulfide.

(total 90 + 239) revealed high concentrations of unknown harmful gases escaping from boreholes #1 and #2. While ensuring that the ventilation system was functioning properly, on-site personnel promptly halted construction to carry out rapid and continuous gas detection.

Based on the detection point of harmful gases, the detected results are shown in Figure 3. The manual detection data indicate that methane is mainly concentrated at the heading face floor arch foot (W6), Borehole #2, and Borehole #3. The highest methane concentration at the heading face was 0.2741%, while the concentration inside the advanced horizontal boreholes reached 100% and remained at this level for over 48 h. This indicates the presence of high methane gas accumulations within the surrounding rock ahead of the heading face. The carbon monoxide (CO) concentration at the heading face reached a maximum of 970 ppm, and no CO detected in the boreholes, likely due to pollution from tunnel vehicles. Hydrogen sulfide (H<sub>2</sub>S) was only detected in Borehole #2 (Figure 7).

#### 4.1.2 Digital Surveillance

During tunnel advance operations, the maximum wind speed at both the heading face and the return air section was 2.2 m/s, exceeding the minimum allowable wind speed of 0.25 m/s (Figure 7). Figure 5 indicates that the maximum methane concentration at the heading face reached 2.43%, developing within approximately 28 h of the advance operation, with an average concentration of 0.093%. Manual detection at point W6 in the heading face recorded a maximum methane concentration of 0.2741%. During drilling, the methane concentration inside the boreholes repeatedly exceeded 0.5%, triggering alarms (Figure 7) (National Railway Administration, 2019).

The concentration of methane at the top of the heading face is significantly higher than in other areas, indicating gas accumulation at the arch. CO monitoring peaked at 10 ppm, while manual detection recorded a peak concentration of 970 ppm, linked to inadequate and untimely treatment of emissions during tunnel construction. No hydrogen sulfide was detected at the heading face, but the on-site detection team found concentrations between 26 and 37 ppm in Borehole #2, suggesting the presence of hydrogen sulfide gas from the borehole. Effective ventilation prevented accumulation, and the hydrogen sulfide likely originates from deeper geological source rocks.

#### 4.1.3 GC characteristics

Gas chromatography separated the volume content of each component in the tunnel based on the different partition principles between the mobile and stationary phases of harmful gases. According to the gas analysis results in Table 2, the composition of hydrocarbon gases released into the tunnel ranged from 28.16% to 47.39%, with methane content varying from 26.15% to 45.16%, reaching a maximum of 45.16%, which exceeds the standard limit by nearly 45 times (National Railway Administration, 2019), with an average of 33.35%. Heavier hydrocarbons (C<sub>2-5</sub>), such as ethane, were relatively low, with a maximum abundance of 2.27% and a minimum of 1.73%, averaging 1.97%. The dryness coefficient of the natural gas in the study area, defined as C<sub>1</sub>/C<sub>2+</sub>, generally ranged from 0.70 to 0.95, except for Borehole #2, which had a value of 0.96 (Zhou et al., 2022). The methane content was less than 95%, indicating the presence of wet gas with a lower degree of thermal evolution.

The non-hydrocarbon gas content in the study area was significantly lower than that of hydrocarbon gases, mainly consisting of nitrogen, carbon dioxide, carbon monoxide, and hydrogen

TABLE 2 Gas detection results measured while drilling at the excavation heading face of the Tingzikou Irrigation District.

Detection time	Location	CH <sub>4</sub>	CO	SO <sub>2</sub>	H <sub>2</sub> S	Remarks
		%	ppm	%	ppm	
2023/7/15	Heading Face (or Tunnel Face)	0.042%	9	0	0	W6
	Borehole #1	0	0	0	0	
	Borehole #2	100%	858	0	26	
2023/7/16	Heading Face	0.022%	9	0	0	W6
	Borehole #1	0	0	0	0	
	Borehole #2	100%	850	0	27	
2023/7/17	Heading Face	0.0095%	0	0	0	W6
	Borehole #1	0	0	0	0	
	Borehole #2	100%	970	0	36	
2023/7/18	Heading Face	0.2741%	10	0	0	W6
	Borehole #1	0.0021%	0	0	0	
	Borehole #2	100%	817	0	37	

TABLE 3 Analysis results of gas components in the advance drilling and overflow point gas chamber experiments.

ID	Sampling location	Gas component content (%)								
		CH <sub>4</sub>	C <sub>2</sub> H <sub>6</sub>	C <sub>3</sub> H <sub>8</sub>	C <sub>4</sub> H <sub>10</sub>	C <sub>5</sub> +	H <sub>2</sub> S	CO	CO <sub>2</sub>	C <sub>1</sub> /C <sub>2+</sub>
WCK1	W6	27.12	1.63	0.32	0.072	0.018	0.004	-	0.04	0.93
WCK2		26.15	1.61	0.32	0.058	0.021	0.004	0.02	0.01	0.93
WCK3		26.16	1.65	0.35	0.051	0.012	0.004	-	0.03	0.93
WCK4		27.27	1.58	0.29	0.059	0.01	0.004	0.02	0.04	0.93
WCK5		26.32	1.52	0.31	0.068	0.023	0.004	0.01	0.03	0.93
WCK6	Borehole #1	45.16	1.75	0.42	0.05	0.01	0.003	-	0.08	0.95
WCK7		37.97	1.44	0.33	0.01	0.01	0.002	-	0.07	0.95
WCK8	Borehole #2	39.4	1.53	0.35	0.03	0.01	0.003	-	0.05	0.95
WCK9		44.58	1.42	0.3	0.03	0.01	0.004	-	0.07	0.96

sulfide. The nitrogen content ranged from 45.7% to 54.9%, with an average of 51.5%. The high nitrogen levels may be influenced by sampling operations and might not accurately reflect the exact composition of detected gases. Carbon dioxide content ranged from 0.01% to 0.08%, while carbon monoxide ranged from 0.01% to 0.02% (Table 3). These low concentrations along with trace amounts of hydrogen sulfide are attributed to acid fracturing during the experiment (Table 3).

#### 4.1.4 Stable isotope characteristics

Carbon isotope is as important geochemical indicator for distinguishing the genesis types of natural gas and have been widely used (Maimaiti et al., 2022). Studies have shown that carbon isotopes of gases is influenced by several factors such as source material type, sedimentary environment, migration processes, and gas maturity. Ethane isotopes, compared to methane isotopes, exhibit greater stability and are less affected by maturity, making them more

effective in reflecting the type of source material (Ojha et al., 2023; Cesar, 2022). Therefore, ethane isotopes are commonly used to determine the origin of natural gas. Previous studies on ethane isotopes suggested that a  $\delta^{13}\text{C}_2$  value of  $-28\text{‰}$  is considered a critical threshold, whereby lower  $\delta^{13}\text{C}_2$  values indicate oil-type gas, while those values higher than  $-28\text{‰}$  also suggest coal-type gas (Lan et al., 2023; Zuo et al., 2023). As shown in Table 4, the isotopic composition of natural gas in the study area exhibits a positive sequence distribution of  $\delta^{13}\text{C}_1 < \delta^{13}\text{C}_2 < \delta^{13}\text{C}_3$ . Methane isotopes are lighter than those of ethane and propane, with values ranging from  $-36.63\text{‰}$  to  $-35.10\text{‰}$ , averaging  $-35.81\text{‰}$ . Ethane isotopic values are in the range of  $-29.53\text{‰}$  to  $-28.11\text{‰}$ , with an average of  $-28.80\text{‰}$ , while propane isotope values range from  $-24.68\text{‰}$  to  $-22.77\text{‰}$ , with an average of  $-24.05\text{‰}$ . The enrichment of ethane ( $\delta^{13}\text{C}_2$ ) varies significantly across different strata. The  $\delta^{13}\text{C}_2$  values are lower than that of the Jurassic Shaximiao Formation and higher than those of the Triassic Xujiahe Formation, with ethane isotopic compositions lower than  $-28\text{‰}$ , indicating oil-type gas.

## 4.2 Source and origin analysis

### 4.2.1 Sources of shallow natural gas

By collecting and analyzing regional geological and geochemical data, it was found that the study area is situated within the Longgang gas-bearing region influenced by the Shuanghe Anticline, Jiulongshan Anticline, and Yilong Anticline structures (Wang et al., 2020). To accurately compare and analyze the source of the harmful gases emerging from the tunnel, the ethane isotope composition characteristics of the central Sichuan and Longgang regions were investigated and compared with the ethane isotope values of this study tunnel.

Previous studies indicated that the Triassic-Jurassic strata in the Sichuan Basin are characterized by high-quality source rocks with significant hydrocarbon generation potential and thermal maturity of preserved organic matter (Hou et al., 2021; Yu et al., 2023). The organic carbon content of the Jurassic Lianggaoshan and Da'anzhai members of the Ziliujing Formation reaches up to 3.01 wt% and 3.7% wt%, respectively, comparable to the Upper Triassic Xujiahe Formation, which contains total organic carbon (TOC) content of up to 3.1 wt% (Qin et al., 2018; Fang et al., 2023). This suggests a very good abundance of organic matter (Peters and Cassa, 1994). Of note, most samples from the aforementioned stratigraphic successions are dominated by hydrogen index values below 200 mg HC/g TOC and  $T_{\text{max}}$  values ranging from  $442^\circ\text{C}$  to  $474^\circ\text{C}$ , indicating that the preserved organic matter is primarily kerogen Type III of gas-prone hydrocarbon with maturation levels varying from the early stage of the oil window to the post-mature stage of dry gas generation (Hou et al., 2021; Yu et al., 2023). These findings reinforce the enhanced generation potential of natural gases that might migrated across porous and permeable pathways into the tunnel area.

Previous geochemical studies of oil and gas data indicate that ethane isotope values transition from  $-35.50\text{‰}$  to  $-21.40\text{‰}$  from the Triassic Leikoupo Formation ( $T_3l^3$ ) to the Jurassic Dongyue Temple Formation ( $J_1d$ ) (Qin et al., 2018). The ethane isotope values ( $\delta^{13}\text{C}_2$ ) of shallow natural gas in the study area range from  $-29.53\text{‰}$  to  $-28.11\text{‰}$ , with an average of  $-28.80\text{‰}$  (Figure 8). These values are similar to the  $\delta^{13}\text{C}_2$  values of  $-30.4\text{‰}$  in the Jurassic Lianggaoshan

Formation ( $J_1l$ ) of the 1HF well and  $-28.20\text{‰}$  in the Jurassic Mianshan Formation ( $J_1m$ ) of the YB10 well (Zhou et al., 2019), but heavier than the average values of  $-29.82\text{‰}$  in the Pearl Chong Formation,  $-31.22\text{‰}$  in the Leikoupo Formation, and those of the Xujiahe Formation. Based on the ethane isotope values as well as the aforementioned Rock-Eval results, the shallow natural gas released into the tunnel area originates from the same underlying the  $J_1l$  and  $J_1m$  formations, specifically from the shallow oil and gas layers of the Jurassic Dazhai Section. The ethane isotope value of  $-30.40\text{‰}$  in the Triassic Xujiahe Formation is the lightest, indicating that faults formed during the Indonesian period may have facilitated gas transport upward. Comparative studies of anomalous harmful gases near the tunnel area reveal the following characteristics (Table 5):

- (1) The tunnel construction crossing the Jurassic Suining Formation ( $J_2s$ ) in central Sichuan, which is a weak red bed with a maximum burial depth of approximately 45.7 m–211 m, resembles the geological and burial depth characteristics of the studied tunnel area.
- (2) In the tunnel gas field, the maximum concentration of methane is 40%, particularly noted in the Muzhu Zhai and Yunwu Zhai tunnels. Gas accumulation can lead to potential combustion incidents, as observed in the Li Jiawan Tunnel and Gan Zi Ping Tunnel (Shijiazhuang Railway University, 2016). This suggests that deep oil and gas from the gas field significantly influence the shallow strata, forming localized enrichments that pose safety risks to tunnel construction.
- (3) Gas tunnels and gas anomaly points near the study area are located in the core region of the Longgang Gas Field, with the overarching structure encompassing the Shui Kou Chang to Yilong, Longgang to Hua Cong, and Shui Jia Cang positive structural belts. Certain concentrations of natural gas in tunnel stratum may be linked to structural faults, allowing the released gas to migrate through the fault system into shallow sandstone bodies, forming independent gas pockets.

### 4.2.2 Origin of alkanes

Methane and other alkane gases can be classified as organic and inorganic based on their origin (Wang et al., 2020; Magdy Lotfy et al., 2022). They can further be divided into coal-bearing strata and hydrocarbon decomposition from oil- and gas-bearing strata, categorized as oil-type gas, coal-type gas, and biogenic gas. Gases from different origins show distinct isotopic differences. Inorganic gases typically have  $\delta^{13}\text{C}_1$  values between  $-25\text{‰}$  and  $-30\text{‰}$  with a negative carbon isotope series, while organic gases have  $\delta^{13}\text{C}_1$  values below  $-25\text{‰}$  with a positive carbon isotope trend (Figure 8). In this study, the methane isotopic values range from  $-36.63\text{‰}$  to  $-35.10\text{‰}$ , averaging  $-35.81\text{‰}$ , which is significantly higher than  $-55\text{‰}$ , thus excluding biogenic gas origin (Figure 8). Additionally, the alkane isotopes exhibit a sequential distribution of  $\delta^{13}\text{C}_1 < \delta^{13}\text{C}_2 < \delta^{13}\text{C}_3$ .

The calculated proxies and relationships of  $\ln(C_1/C_2)$  and  $\ln(C_2/C_3)$  were plotted using the genetic type identification diagram (Figure 9). With increasing thermal maturity, oil cracking gas tends to stabilize, while gas from kerogen cracking continues to increase. The component characteristics and alkane isotope relationships of the shallow natural gas indicate that ethane isotope values in the

TABLE 4 Shows the quantitative distribution of  $\delta^{13}C_1$ ,  $\delta^{13}C_2$  and  $\delta^{13}C_3$  isotope values in central Sichuan area.

Location	Stratum	Carbon isotope ‰			Remarks
		$\delta^{13}C_1$	$\delta^{13}C_2$	$\delta^{13}C_3$	
Central Sichuan	J <sub>2</sub> s	-39.21~-28.20	-32.76~-21.80	-29.14~-18.52	Yang (2021)
J61-4		-38.2	-31.8	-22.8	Xia et al. (2019)
J62		-37.70	-32.80	-22.90	
J63-1		-37.60	-32.10	-22.90	
J63-2		-37.90	-31.70	-22.90	
LG18		-43.50	-36.80	-30.00	
1HF	J <sub>1</sub> l	-42.20	-30.40		Experiments in This Paper
Study Area		-36.13	-29.35	-23.90	
		-35.35	-29.53	-22.77	
		-36.07	-28.11	-24.68	
		-35.10	-28.19	-24.18	
		-36.63	-28.85	-24.68	
		-35.61	-28.74	-24.08	
YB10	J <sub>1</sub> m	-31.20	-28.20	-29.00	Liu et al. (2011)
YB02	J <sub>1</sub> d	-37.00	-21.40		
YB03		-38.30	-24.30	-22.30	
YB04	J <sub>1</sub> z	-33.90	-24.40	-23.90	Zhang et al. (2023a)
LG2		-47.60	-33.00	-28.10	
LG7		-47.50	-32.30	-27.70	
LG42		-46.00	-33.20	-28.70	
LG18		-40.70	-26.20	-22.70	
YB05	T <sub>3</sub> x	-31.10	-30.40	-24.90	Liu et al. (2011)
YB05		-32.00	-27.00	-23.40	
LG18	T <sub>2</sub> l <sup>4</sup>	-36.50	-35.50	-30.50	Zhang et al. (2023a)
LG176	T <sub>2</sub> l <sup>4</sup>	-37.80	-32.50	-30.60	
Zhong18	T <sub>2</sub> l <sup>3</sup>	-35.20	-30.20	-30.10	This study
Zhong 46		-34.20	-29.30	-27.50	
Zhong 81		-34.20	-28.60	-26.80	

study area are below -28.0‰, suggesting that the organic matter is in the mature to post-mature stages, with vitrinite reflectance (Ro%) values in the range of 1.05%–1.1% and that the gas is formed through high-temperature cracking (Peters and Cassa, 1994). These findings

are consistent with the Rock-Eval T<sub>max</sub> values that ranging from 442°C to 474°C, indicating that the preserved organic matter is in the oil window to post-mature stages of dry gas generation (Peters and Cassa, 1994; Hou et al., 2021; Yu et al., 2023).

TABLE 5 Gas anomaly characteristics in the adjacent tunnel area.

Gas anomaly zone	Type of escaping gas	Maximum concentration (%)	Maximum burial depth (m)	Explanation
MZZ Tunnel	CH <sub>4</sub>	40	77	Combustion
YWZ Tunnel	CH <sub>4</sub> 、CO	40	211	Water Accumulation and Bubbling
LJW Tunnel	Shallow Natural Gas	0.28	95	Combustion, 1 person injured 伤
GZP Tunnel	CH <sub>4</sub>	—	148	Combustion
NQY Tunnel	CH <sub>4</sub>	0.46	188	—
MPS Tunnel	CH <sub>4</sub>	0.0168	160	Low concentration
TSS Tunnel	CH <sub>4</sub>	0.95	160	High concentration
LLS Tunnel	CH <sub>4</sub>	0.0144	45.7	Low concentration
YSZ Tunnel	CH <sub>4</sub> 、H <sub>2</sub>	0.0356	146.55	Low concentration
Anomaly Point #1	CH <sub>4</sub> 、H <sub>2</sub> S、CO	—	100	Foul Odor
Anomaly Point #2	CH <sub>4</sub> 、H <sub>2</sub> S、CO	1.14	—	Combustion
Anomaly Point #3	Unknown Gas	—	60	Blowout

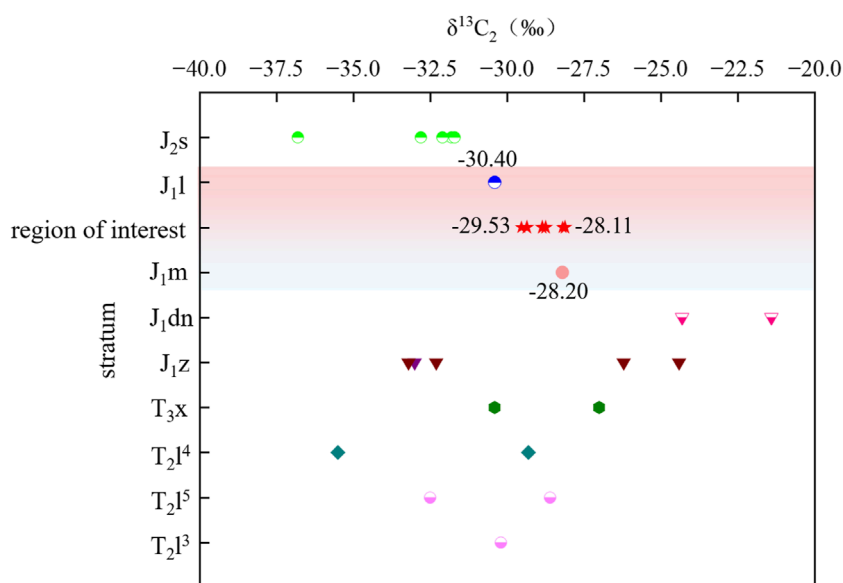
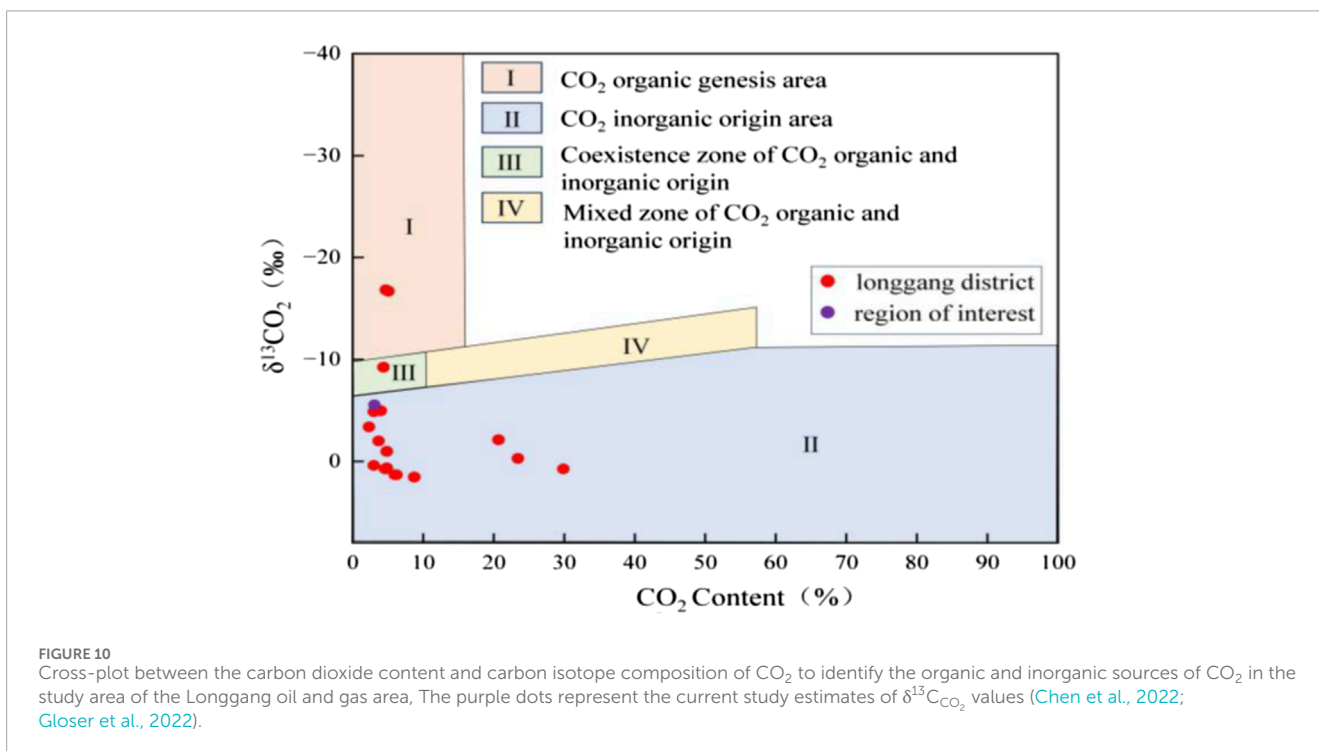
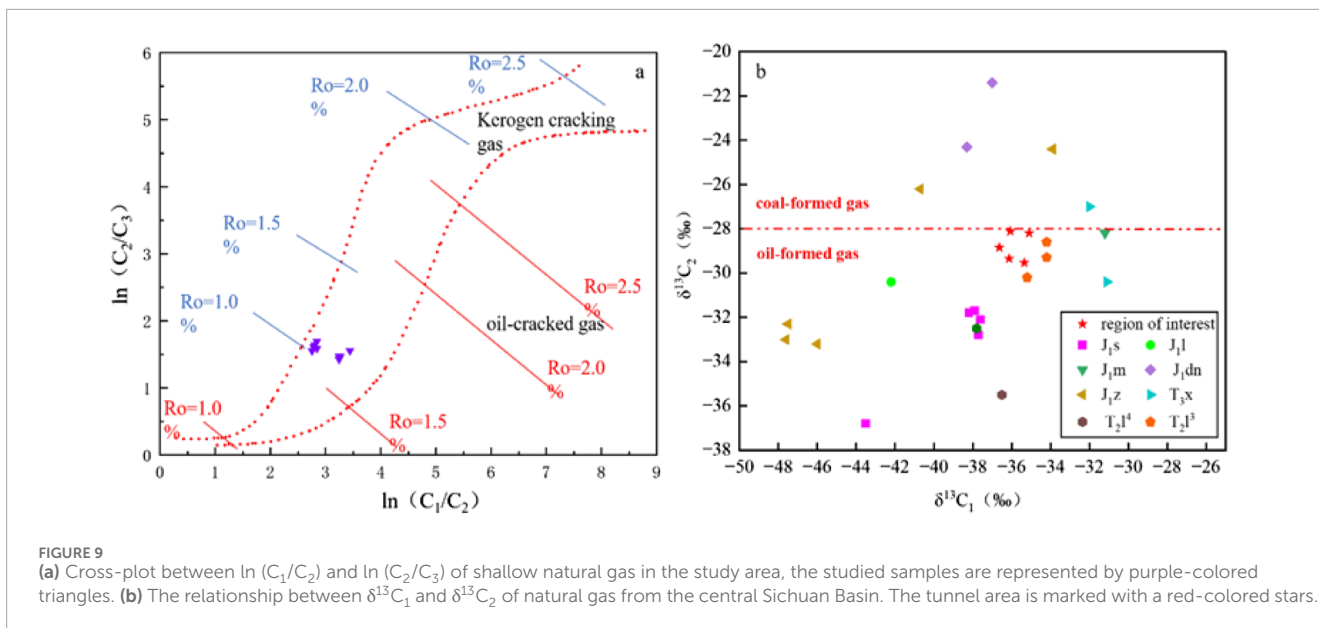


FIGURE 8 Comparison of ethane isotope values between shallow natural gas in the study area and source rocks in central Sichuan. The tunnel body stratum is J<sub>2</sub>s, and the ethane isotope values are between J<sub>1</sub>m and J<sub>1</sub>l (Yang, 2021; Zhang B. et al., 2023).

Notably, the Upper Triassic-Jurassic Xujiahe (T<sub>3</sub>x) and Pearl Chong (J<sub>1</sub>z) formations contain coal-type gases. Geological data indicate that the tunnel is situated above the Longgang Gas Field, with abundant gas sources released from mature source rocks. The developed fault system and structural movements have caused oil and gas to diffuse from high-pressure source

rock areas to low-pressure shallow strata. Gas concentration testing at the tunnel exit and boreholes shows that methane volume content ranges from 26.16% to 45.16% along with heavier hydrocarbons such as ethane and propane. Therefore, it is concluded that the hydrocarbon gases in this tunnel space are organic oil-type gas.



### 4.2.3 Hydrogen sulfide genesis

Hydrogen sulfide ( $H_2S$ ) gas is a severe neurotoxin that can damage the eyes and respiratory system when its concentration exceeds the maximum permissible limit of 0.00066%. Studying the origin of  $H_2S$  in shallow natural gas is crucial to ensure the safety of construction personnel (Li et al., 2016). There are four main sources of hydrogen sulfide, including biogenic decomposition, bacterial sulfate reduction, thermochemical sulfate reduction, and magmatic activity (Dai et al., 2018; Cheng et al., 2022; Gopinathan et al., 2022; Gilbert et al., 2022). The concentration of  $H_2S$  released from the biological decomposition of sulfur-containing

organic matter rarely exceeds 3%, with  $\delta^{34}S$  values around 15‰. Gas derived from bacterial sulfate reduction is formed under dissimilatory reduction in an anaerobic environment below 80°C, typically containing less than 2%  $H_2S$ . Thermochemical sulfate reduction processes can yield  $H_2S$  concentrations of less than 1%, which are often considered the primary source of sulfur-containing gas reservoirs in the petroleum industry. Geological and geochemical data from the study area indicate trace amounts of sulfur detected in some exploration wells in the Longgang Gas Field. Additionally, proximity of the study area to the Puguang Gas Field, known for high-sulfur carbonate rocks, provides sufficient reactants.

Thus, the predominant source of toxic H<sub>2</sub>S gas in the tunnel area is likely generated through thermochemical sulfate reduction.

#### 4.2.4 Carbon dioxide and carbon monoxide genesis

The origin of carbon dioxide (CO<sub>2</sub>) in the central Sichuan region is attributed to both organic and inorganic sources. Organic sources are akin to those found in oil and gas reservoirs, while inorganic origins include biological processes, mantle degassing, and rock chemical reactions (Menoud et al., 2022; Pearce et al., 2023). Changes in the carbon isotope composition of CO<sub>2</sub> ( $\delta^{13}\text{C}_{\text{CO}_2}$ ) can be used as reliable indicator to distinguish between organic and inorganic sources. Data compilation of  $\delta^{13}\text{C}_{\text{CO}_2}$  reveal that  $\delta^{13}\text{C}_{\text{CO}_2}$  values greater than  $-8\text{‰}$  indicate an inorganic origin, while values generally below  $-10\text{‰}$  suggest an organic origin. Based on the CO<sub>2</sub> gas composition from the tunnel and the  $\delta^{13}\text{C}_{\text{CO}_2}$  characteristics in the Longgang oil and gas area of central Sichuan, a diagram was created to differentiate between the organic and inorganic origins of CO<sub>2</sub>.

Most CO<sub>2</sub> samples are of inorganic origin, where CO<sub>2</sub> concentrations in the shallow natural gas at the tunnel site ranging from 0.01% to 0.08%. This suggest a  $\delta^{13}\text{C}_{\text{CO}_2}$  value of less than  $-8\text{‰}$ , indicating it is Class II inorganic gas, formed by the thermal decomposition of carbonate rocks. Carbon monoxide (CO) poses serious health risks by binding to hemoglobin in the blood, preventing hemoglobin oxygen transport, and leading to can cause asphyxiation and death 17. It results from incomplete oxidation of carbon-based fuels or geological activities, such as volcanic eruptions. Tectonic movements have caused uplifts and the formation of multiple sets of faults, which can facilitate the production and storage of CO from deeper layers stored in pockets of strata. Additionally, gases generated from explosives used in tunnel excavation can contain approximately 30%–60% CO, while exhaust gases from diesel and gasoline engines can include about 1%–8% CO. Inadequate tunnel ventilation or distant exhaust outlet hinder CO dispersion, leading to a mixed origin of the measured CO (Table 3).

#### 4.3 Implications for shallow natural gas disasters in hydrocarbon-bearing regions

Investigating the causes of shallow natural gas disasters in oil- and gas-bearing regions, a comprehensive dataset was compiled from adjacent tunnel engineering projects within the central Sichuan region. This area is known for multiple occurrences of harmful gas escape incidents. These events have predominantly affected tunnel infrastructures associated with railway, highway, and hydraulic engineering projects (Chen et al., 2022; Qiu et al., 2025). The detection and monitoring during tunnel construction show that the main component of shallow natural gas is methane, with less carbon monoxide and hydrogen sulfide. According to the buried depth of the construction project, formation lithology and oil and gas fields, a total of 31 datasets from 18 tunnel projects were systematically collected and analyzed (Table 6). The data analysis reveals a significant correlation between shallow natural gas escape of the tunnel and both the lithological composition and tectonic settings of the surrounding formations.

The data showed that the escape concentrations exhibit a distinct three distribution pattern. High-value zones (>70,000 ppm) are primarily concentrated in the Ganziping and JLSLSD tunnels within the Longgang Oil and Gas Field. These sites are dominated by interbedded mudstone and sandstone, with gas releases sometimes accompanied by combustion phenomena, suggesting intense gas migration and accumulation. Medium-to high-value zones (5,000–10,000 ppm) are mainly developed in sandstone-dominated strata, as observed in the Xuanpengling and Sifangshan tunnels. These escapes typically occur at depths of 200–400 m, and show a strong positive correlation with maximum burial depth. In contrast, low-value zones (<1,000 ppm) tend to occur in shallower formations dominated by argillaceous sandstone, with gas escapes often confined to depths shallower than 150 m.

The data of multiple groups in Longgang oil and gas field show that the high escape concentration is closely related to the mudstone-sandstone interbedded structure, and the anomaly value of DZZSD-3# reaches 50,000 ppm at a buried depth of 226.6 m, which may indicate the existence of a hidden fault zone and is of great significance for deep gas transportation. These rules highlight the key role of lithological assemblage and burial depth parameters in the natural gas migration model, that is, the sand and mudstone formations have almost no gas production capacity, and the tunnel or tunnel engineering with shallow natural gas outburst is located in the oil and gas pointing area, which further indicates that the shallow natural gas in the tunnel construction project is developed from the deep to the upward part through the fault system.

#### 4.4 Possible scenarios of migration patterns

The shallow natural gas found in tunnel spaces primarily consists of high concentrations of methane, with lower levels of carbon monoxide, carbon dioxide, and trace amounts of hydrogen sulfide. The tunnel passes through the Suining Formation, which lacks the capacity to generate hydrocarbons. The shallow secondary gas reservoirs in the central Sichuan Basin originated from various hydrocarbon source rocks, including the Upper Triassic Xujiahe Formation and the Lower Jurassic dark mudstone of the Lianggaoshan and Da'anzhai members of the Ziliujing Formation. The coal seams of the Upper Triassic Xujiahe Formation, occurs at high burial depth of >1,000 m, underwent hydrocarbon generation during the Early Indosinian period (Zhang X. et al., 2023). However, as tectonic faults in the underlying Jurassic formations gradually diminish, and due to incomplete communication of reservoir gas with upper formations via deep major faults, gas migration and replenishment to the upper rock layers, including the tunnel formations, are challenging.

The reservoir rock properties in the Sichuan Basin are relatively poor, with deep gas migration occurring not only through rock mass conduits, but also via fault or joint-fracture systems. Gas tunnels in non-coal formations are classified into three types based on the rock characteristics: structurally connected type, metamorphic surrounding rock type, and composite genetic type (Kang et al., 2013). Based on regional geological and 3D seismic data from the petroleum sector, we observed that faults at the bottom boundaries of the Jurassic Zhenzhuchong and Shaximiao formations

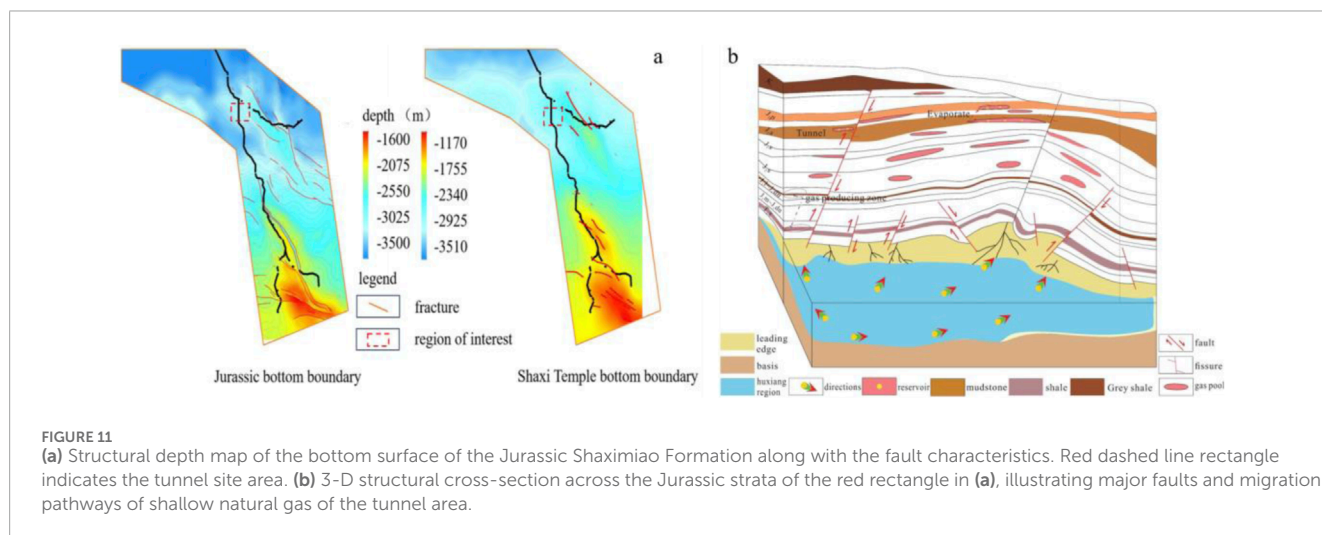
TABLE 6 Gas anomaly characteristics in the adjacent tunnel area.

No	Name	Length	Maximum burial depth	Escape concentration	Escape depth	Cavity section stratum	Oil and natural gas fields	Remark
		m	m	ppm	m			
1	Ganziping	1377	148	>70000		Mudstone, sandstone, siltstone	Longgang	Combustion
2	Xuanpanling	5986	500	5000	246	Sandstone	Hewancahng	
3	Xuanpanling	5986	500	6030	430	Sandstone	Hewancahng	
4	Xuanpanling	5986	500	7500	265	Sandstone	Hewancahng	
5	Meilinguan	8275	102.21	4305	405	Sandstone	Shejianhe	Bubble escape
6	Meilinguan	8275	405	9740	67	Sandstone	Shejianhe	Bubble escape
7	Sifangshan	7860	-	6500	102	Sandstone	Yuanba	
8	Sifangshan	7860	-	2730	345	Sandstone	Yuanba	
9	Xiaojialiang	5159	96	2300	79.05	Sandstone	Yuanba, Jiulongshan	Bubble escape
10	Xiaojialiang	5159	96	8730	156	Sandstone	Yuanba, Jiulongshan	Bubble escape
11	Xiaojialiang	5159	96	8130	75	Fine sandstone	Yuanba, Jiulongshan	Bubble escape
12	Mingjuesi	5736	350	9510	405	Sandstone	Shejianhe	
13	Xuanzhenguan	7554	302.14	3830	240.2	Sandstone	Shejianhe	
14	Sifangshan	7860	102	6500	102	Sandstone	Hewancahng	
15	Sifangshan	7860	345	2730	345	Sandstone	Hewancahng	
16	Tushansi	3216	160	640000		Mudstone clamp sandstone	Longgang	
17	Lujiaju	4714	152	33600	90	Mudstone clamp sandstone	Yuanba	
18	Lujiaju	4714	153	35200	118	Mudstone clamp sandstone	Yuanba	
19	Lujiaju	4714	154	35200	150	Mudstone clamp sandstone	Yuanba	
20	Laolinshan	561	45.7	144	65	Argillaceous sandstone	Gongshanmiao	
21	Taipengshan	842	142	358	80	Argillaceous sandstone	Gongshanmiao	
22	Chibashan4#	1884	-	43	56	Mudstone, siltstone	Longgang	
23	Chibashan4#	1884	-	83	92	Mudstone, siltstone	Longgang	
24	Chibashan4#	1884	-	100	128	Mudstone, siltstone	Longgang	
25	Chibashan4#	1884	-	100	158	Mudstone, siltstone	Longgang	

(Continued on the following page)

TABLE 6 (Continued) Gas anomaly characteristics in the adjacent tunnel area.

No	Name	Length	Maximum burial depth	Escape concentration	Escape depth	Cavity section stratum	Oil and natural gas fields	Remark
		m	m	ppm	m			
26	Yanshanzhai	1898	146.55	356	123	Sandy mudstone	Longgang	
27	Yanshanzhai	1898	146.55	105	57	Sandy mudstone	Longgang	
28	DZZSD-3#	7129	226.6	50000	205	Sandstone-mudstone	Longgang	
29	JJLSD	4282	163.4	>70000	160	Sandstone-mudstone	Longgang	
30	YHZSD	2590	155	冒泡	150	Sandstone-mudstone	Longgang	
31	CGLSU	9729	312	100	311.5	Sandstone-mudstone	Longgang	



primarily develop in the southern and northeastern parts of the Jurassic system adjacent to the tunnel layer. These faults are about 1–3 km in length, and extends up to 10 km in length (Figure 11). These faults in both regions occur across an anticline structure, with their spatial positions roughly overlapping with the Yilong, Shuanghechang, and Yingshan anticlines. Comprehensive analysis suggests that the shallow harmful gases originate from the structurally connected type, which has a certain impact on the studied tunnel.

The underlying Da’anzhai Member in this area is rich in oil and gas resources. The faults associated with syncline and anticline structures near the tunnel site, combined with numerous fractures that facilitate gas transport, create pathways for the accumulation and migration of shallow natural gas. As illustrated in Figure 11, these fault-controlled structures and the heterogeneous fracture-porosity network enable the generate gases from the Da’anzhai Member source rocks in the Jurassic Ziliujing Formation to migrate upward into the shallow fractures and porous sandstones. The

sandstone interlayer is widely distributed in the tunnel chambers, comprised fine, dense particles with moderate porosity, which forms a shallow reservoir with significant variations in capacity and distribution, resulting in accumulations of shallow gas pockets. However, construction activities disturb this layer with further fractures, joints, and fissures, which facilitating the release of harmful natural gases into the tunnel space. Consequently, this poses challenges to maintaining normal construction operations in the tunnel.

### 4.5 Safety prevention and control

It is essential to conduct regular inspections and maintenance of all equipment that may produce toxic gases to ensure they operate under safe conditions. Timely safety measures for gas poisoning should be implemented for on-site personnel, and emergency evacuation and rescue plans must be established to address

any abnormal gas occurrences or combustion events. For long-distance tunnels with small cross-sections, the strategic placement of ventilation ducts and methods can effectively manage the diffusion and concentration of toxic and harmful gases. A combination of forced air intake and extraction fans should be installed on both sides of the tunnel walls. Localized ventilation should be enhanced in areas prone to gas accumulation and ventilation blind spots. Following blasting operations, ventilation should continue for at least 20 min before personnel can safely enter the tunnel wearing oxygen-supplied gas masks to resume work.

Traditional ventilation and surface sealing methods are often ineffective for dissipating and containing harmful gases with unclear release points. Chemical absorption reactions are vital for reducing or preventing the combustion or explosion of toxic gases. Understanding the physical and chemical properties of carbon monoxide (CO), methane (CH<sub>4</sub>), and hydrogen sulfide (H<sub>2</sub>S) present in the tunnel is crucial. Utilizing NaOH-containing water mist and high-surface-area activated carbon can aid in removing and adsorbing certain toxic gases, such as carbon monoxide and hydrogen sulfide. When managing high concentrations of methane, it is critical to minimize reliance on ventilation. The most effective approach to mitigate methane hazards in tunnels involves employing extraction methods, using mechanical equipment and specialized pipelines to safely extract and discharge residual or released methane to a secure location under negative pressure, where it can be repurposed as fuel. This strategy not only optimizes the tunnel environment but also enhances economic benefits.

To ensure the safety of the work area, monitoring sensors should be installed based on the characteristics of harmful gas emissions and the specific construction methods employed. These sensors will enable on-site personnel to make timely decisions and necessary adjustments. Monitoring points should be strategically positioned in various locations, including the working face, lining trolley, return air corners, and ventilation blind spots such as the arch crown, arch waist, and arch foot. Because methane is lighter than air, sensors for methane should be positioned at the arch crown. Carbon monoxide sensors, which have a similar molecular weight to air, should also be placed at the arch crown. Conversely, since hydrogen sulfide is heavier than air, its sensors should be located at the arch foot. Additionally, wind speed sensors should be suspended at the top of the tunnel's central axis to ensure adequate air exchange between the tunnel interior and exterior.

Considering the risk factors associated with this tunnel project, it is important to assess geological conditions ahead of the working face and monitor harmful gas concentrations using a combination of advanced drilling and deepened blast holes. Blast holes should be arranged in an isosceles triangle pattern, with each hole reaching a minimum depth of 5 m, drilled at a 45° angle along the tunnel axis. Advanced drilling should be focused at the working face, with horizontal holes extending no less than 50 m deep.

## 5 Conclusion

In response to the shallow natural gas outburst encountered during tunnel excavation for the Tingzikou Water Diversion Project, this study integrates gas composition analysis, stable carbon isotopes, and regional oil and gas data. By drawing analogies

with relevant engineering case studies, the following conclusions are derived:

- (1) The shallow natural gas outflow from the tunnel is primarily methane-based, classified as wet gas with a low thermal evolution degree.
- (2) The analytical data reveal that the majority of carbon dioxide present in the tunnel environment is of inorganic origin (Type II inorganic genetic gas). Conversely, carbon monoxide exhibits characteristics of a mixed genesis, implying contributions from both organic and inorganic sources. Hydrogen sulfide is primarily the result of thermochemical sulfate reduction processes occurring under high-temperature conditions in the subsurface.
- (3) The  $\delta^{13}\text{C}_2$  values in the study area closely align with those recorded for the Jurassic Lianggaoshan Formation (J<sub>1</sub>l) and the Mianshan Formation (J<sub>1</sub>m), while showing a distinct difference from the isotope signature of the deeper Xujiahe Formation. These results suggest that the shallow natural gas originates from the Da'anzhai Member of the Ziliujing Formation. This supports the interpretation that the gas is the result of an “*in-situ* generation and storage” mechanism, whereby hydrocarbons are formed and retained within the same stratigraphic unit without significant lateral migration.
- (4) Deep-source gases appear to migrate and accumulate in permeable sandstone reservoirs via structural pathways, such as fractures or joints, fissures, and faults, which serve as conduits connecting deeper hydrocarbon systems to shallower formations. Construction activities may disturb these structural networks, causing gas-rich zones, often existing as isolated pockets, to discharge abruptly into tunnel spaces through these pre-existing migration channels, leading to localized gas accumulation and potential outbursts.

This study focuses on a large-scale construction project and explores the origin of shallow natural gas in hydro-engineering tunnels located in structurally complex oil and gas regions. By identifying the gas source and clarifying the upward migration pathways, the findings serve as a valuable reference for the fieldwork planning and risk assessment. Furthermore, the controlling mechanisms of gas migration and accumulation within such tunnel environments remain of ongoing research, particularly in enhancing safety protocols and predictive modeling for future tunnel construction in hydrocarbon-bearing regions.

## Data availability statement

The original contributions presented in the study are included in the article/supplementary material, further inquiries can be directed to the corresponding authors.

## Author contributions

SW: Conceptualization, Formal Analysis, Investigation, Project administration, Supervision, Visualization, Writing – original draft. XG: Data curation, Resources, Software, Validation, Visualization, Writing – original draft. PS: Funding acquisition, Methodology,

Supervision, Validation, Writing – review and editing. LL: Data curation, Investigation, Methodology, Resources, Software, Validation, Writing – review and editing. MA: Funding acquisition, Resources, Validation, Writing – review and editing. XC: Data curation, Investigation, Methodology, Resources, Visualization, Writing – review and editing. XZ: Conceptualization, Data curation, Formal Analysis, Methodology, Project administration, Resources, Writing – review and editing. TG: Project administration, Validation, Visualization, Writing – review and editing. AM: Funding acquisition, Supervision, Validation, Writing – review and editing.

## Funding

The author(s) declare that financial support was received for the research and/or publication of this article. The authors declare funding from the Sichuan Science and Technology Plan Project (No. 2024ZDZX0009), National Natural Science Foundation of China (W2433105), Shallow natural gas hazard evaluation system and key prevention and control technologies of tunnel group in oil and gas bearing basin (0-JF-2023- Tingzikou Irrigation District-0-2), and the Ongoing Research Funding program, (ORF-2025-455), King Saud University, Riyadh, Saudi Arabia.

## Acknowledgments

The authors thank the Tingzikou Irrigation District Water Diversion Construction Project and the key prevention and control technologies of the oil and gas basin tunnel group for their support to conduct this work. Sichuan Water Development Survey and Design Institute and China Railway 18<sup>th</sup> Bureau provided assistance in

## References

- Adsul, T., Ghosh, S., Kumar, S., Tiwari, B., Dutta, S., and Varma, A. K. (2023). Biogeochemical controls on methane generation: a review on Indian coal resources. *Minerals* 13 (695), 695. doi:10.3390/min13050695
- Aharon, P., Platon, E., and Sen Gupta, B. K. (2022). An assessment of foraminiferal species distribution and stable-isotope anomalies at a methane-hydrate mound in the Gulf of Mexico. *J. Palaeontol. Soc. India* 67 (1), 126–138. doi:10.1177/0971102320220111
- Araizaga, A. E., Mancila, Y., and Mendoza, A. (2013). Volatile organic compound emissions from light-duty vehicles in monterrey, Mexico: a tunnel study. *Int. J. Environ. Res.* 7 (2), 277–292. doi:10.1016/j.envsoft.2012.08.007
- Bai, X., Li, J., Zhang, D., Wang, Y., Lu, S., Sui, L., et al. (2024). Geological characteristics and enrichment conditions of shale oil of jurassic Lianggaoshan Formation in yilong-pingchang area, Sichuan Basin. *Lithol. Reserv.* 36 (2), 52–64. doi:10.12108/yxyqc.20240206
- Cesar, J. (2022). Unconventional gas geochemistry—an emerging concept after 20 Years of shale gas development? *Minerals* 12 (10), 1188. doi:10.3390/min12101188
- Chen, D., and Su, P. (2019). Study on the characteristics and hazards of harmful gases in Kanglin section of Sichuan-Tibet Railway. *Railw. Eng. J.* 36 (6), 18–22. doi:10.3969/j.issn.1006-2106.2019.06.005
- Chen, H., Tian, W., Chen, Z., Zhang, Q., and Tao, S. (2022). Genesis of coalbed methane and its storage and seepage space in baode block, eastern ordos basin. *Energies* 15 (1), 81. doi:10.3390/en15010081
- Cheng, Y., Cheng, Y., Feng, Z., Guo, C., Chen, P., Tan, C., et al. (2022). Links of hydrogen sulfide content with fluid components and physical properties of carbonate gas reservoirs: a case study of the right bank of amu darya, Turkmenistan. *Front. Earth Sci.* 10, 910666. doi:10.3389/feart.2022.910666
- sample collection and data collection. The authors acknowledge the Ongoing Research Funding Program Supporting Project number (ORF-2025-455), King Saud University, Riyadh, Saudi Arabia. We thank the associate editor Yuan-Pin Chang and two reviewers for their valuable comments that improved the manuscript.

## Conflict of interest

Author LL was employed by Sichuan Water Development Investigation, Design & Research Co., Ltd. Authors XC and XZ were employed by China Railway 18th Bureau Group Corporation, Ltd. Author TG was employed by Core Laboratories LP.

The remaining authors declare that the research was conducted in the absence of any commercial or financial relationships that could be construed as a potential conflict of interest.

## Generative AI statement

The author(s) declare that no Generative AI was used in the creation of this manuscript.

## Publisher's note

All claims expressed in this article are solely those of the authors and do not necessarily represent those of their affiliated organizations, or those of the publisher, the editors and the reviewers. Any product that may be evaluated in this article, or claim that may be made by its manufacturer, is not guaranteed or endorsed by the publisher.

Copur, H., Cinar, M., Okten, G., and Bilgin, N. (2012). A case study on the methane explosion in the excavation chamber of an EPB-TBM and lessons learnt including some recent accidents. *Tunn. Undergr. Space Technol.* (1), 159–167. doi:10.1016/j.tust.2011.06.009

Dai, J., Ni, Y., Qin, S., Huang, S., Peng, W., and Han, W. (2018). Geochemical characteristics of ultra-deep natural gas in Sichuan Basin. *Petroleum Explor. Dev.* (4), 588–597. doi:10.1016/S1876-3804(18)30067-3

Ding, H., Mo, Xu, and Yue, Z. (2018). Geological characteristics and distribution patterns of harmful gases on the chengdu-guiyang railway. *Sci. Technol. Eng.* (5), 309–314. doi:10.3969/j.issn.1671-1815.2018.05.053

Fang, R., Jiang, Y., Yang, C., Wang, Z., Sun, S., Zhu, X., et al. (2023). Geological characteristics of shale oil in jurassic Lianggaoshan Formation, Sichuan Basin. *China Pet. Explor.* 28 (4), 66–78. doi:10.3969/j.issn.1672-7703.2023.04.007

Gilbert, A., Nakagawa, M., Taguchi, K., Zhang, N., Nishida, A., and Yoshida, N. (2022). Hydrocarbon cycling in the tokamachi mud volcano (Japan): insights from isotopologue and metataxonomic analyses. *Microorganisms* 10 (7), 1417. doi:10.3390/microorganisms10071417

Gloser, J., Friess, J., and Luniaczek, T. (2022). CO<sub>2</sub> reduction in tunnelling from the point of view of construction design and implementation. *Geomechanics Tunn.* 15 (6), 792–798. doi:10.1002/geot.202200045

Gopinathan, P., Jha, M., Singh, A. K., Mahato, A., Subramani, T., Singh, P. K., et al. (2022). Geochemical characteristics, origin and forms of sulphur distribution in the Talcher coalfield, India. *Fuel* 316, 123376. doi:10.1016/j.fuel.2022.123376

Guo, F.-Q., Liang, Y.-Z., Huang, L.-F., and Xu, C.-J. (2004). GC-MS combined with orthogonal projection method or progressive window orthogonal projection method for the determination of volatile oil components in Notopterygium incisum. *J. Chem. High. Educ.* (3), 430–435. doi:10.3321/j.issn:0251-0790.2004.03.008

- Hou, G., Song, B., Ni, C., Chen, W., Wang, L., Yang, D., et al. (2021). Characteristics of tight oil source-reservoir configuration and its significance for oil and gas exploration - a case study of the Jurassic Da'anzhai Member in the central Sichuan Basin. *Sediment. J.* 39 (5), 1078–1085. doi:10.14027/j.issn.1000-0550.2020.122
- Huang, H., Wen, H., Wen, L., Zhang, B., Zhou, G., He, Y., et al. (2023). Multistage dolomitization of deeply buried dolomite in the lower cambrian canglangpu formation, central and northern Sichuan Basin. *Mar. Petroleum Geol.* 152, 106261. doi:10.1016/j.marpetgeo.2023.106261
- Jiang, Y. (2019). *Study on karst reservoir of weathering crust of middle triassic Leikoupo Formation in Longgang area, central sichuan*. Beijing: China University of Petroleum.
- Kang, X. B., Xu, M., Luo, S., and Xia, Q. (2013). Study on formation mechanism of gas tunnel in non-coal strata. *Nat. Hazards* 66 (2), 291–301. doi:10.1007/s11069-012-0484-y
- Lan, H., Tsunogai, U., Nakagawa, F., Ito, M., Shingubara, R., Miyoshi, Y., et al. (2023). Tracing the sources of excess methane in Ise and Mikawa bays using dual stable isotopes as tracers. *Geochem. Journal* 57 (2), 59–72. doi:10.2343/geochemj.gj23005
- Li, P., Hao, F., Guo, X., Zou, H., Zhu, Y., Yu, X., et al. (2016). Origin and distribution of hydrogen sulfide in the Yuanba gas field, Sichuan Basin, Southwest China. *Mar. Petroleum Geol.* 75, 220–239. doi:10.1016/j.marpetgeo.2016.04.021
- Li, P.-J., Chen, C.-S., Chang, H.-P., Ho, H.-H., and Xie, B. (2020). Explosion mechanism analysis during tunnel construction in the Zengwen Reservoir. *Tunn. Undergr. Space Technol.* 97, 103279. doi:10.1016/j.tust.2019.103279
- Liu, R., Guo, T., and Shao, M. (2011). Source and genetic type of shallow natural gas in Yuanba area, Northeast Sichuan. *Nat. Gas. Ind.* (6), 34–38. doi:10.3787/j.issn.1000-0976.2011.06.005
- Liu, K., Chen, J., Tang, S., Zhang, J., Fu, R., Chen, C., et al. (2024). Differential enrichment mechanism of helium in the Jinjia gas field of Sichuan Basin, China. *Mar. Petroleum Geol.* 167, 106970. doi:10.1016/j.marpetgeo.2024.106970
- Magdy Lotfy, N., Qteishat, A., Farouk, S., Ahmad, F., Al-Kahtany, K., and Hsu, C. S. (2022). Geochemical characteristics and genetic types of Ordovician tight gas in the Risha Gas Field, Eastern Jordan based on carbon and hydrogen isotope compositions. *Mar. Petroleum Geol.* 143, 105810. doi:10.1016/j.marpetgeo.2022.105810
- Maimaiti, A., Wang, Q., Hao, F., Yang, X., Zhang, H., and Tian, J. (2022). Oil pyrolysis with carbonate minerals: implications for the thermal stability of deep crude oil. *Mar. Petroleum Geol.* 146, 105929. doi:10.1016/j.marpetgeo.2022.105929
- Menoud, M., van der Veen, C., Maazallah, H., Hensen, A., Velzeboer, I., van den Bulk, P., et al. (2022). CH<sub>4</sub> isotopic signatures of emissions from oil and gas extraction sites in Romania. *Elementa Sci. Anthropocene* 10 (1), 00092. doi:10.1525/elementa.2021.00092
- National Railway Administration (2019). *Technical specification for railway gas tunnels*. National Railway Administration.
- Ojha, S., Punjra, N. K., Chakraborty, A., and Singh, P. K. (2023). Evolution and evaluation of coal-bed methane in cambay basin, western India: insights from stable isotopic and molecular composition. *J. Geol. Soc. India* 99 (2), 193–204. doi:10.1007/s12594-023-2287-z
- Pearce, J. K., Hofmann, H., Baublys, K., Golding, S. D., Rodger, I., and Hayes, P. (2023). Sources and concentrations of methane, ethane, and CO<sub>2</sub> in deep aquifers of the surat basin, great artesian basin. *Int. J. Coal Geol.* 265, 104162. doi:10.1016/j.coal.2022.104162
- Pearson, C. F. C., Edwards, J. S., and Durucan, S. (1992). Methane occurrences in the Carsington aqueduct tunnel project - a case study. in Proc 1989 rapid excavation and tunnelling conference. Los Angeles: Society for Mining, Metallurgy and Exploration.
- Peters, K. E., and Cassa, M. R. (1994). Applied source rock geochemistry. in *The petroleum system - from source to trap*. Editors L. B. Magoon, and W. G. Dow (Memoir: American Association of Petroleum Geologists), 60, 93–120. doi:10.1306/m60585c5
- Qian, T., Li, W., and Liu, S. (2023). Early to middle jurassic sedimentation within the northern Sichuan Basin in response to exhumation of the south qinling orogenic belt, central China. *Palaeogeogr. Palaeoclimatol. Palaeoecol.* 630, 111805. doi:10.1016/j.palaeo.2023.111805
- Qin, S. F., Zhou, Z., Zhou, Z., Yang, Y., and Yang, Y. (2018). Geochemical characteristics of natural gases from different petroleum systems in the Longgang gas field, Sichuan Basin, China. *Energy Explor. Exploitation* 36 (6), 1376–1394. doi:10.1177/0144598718763902
- Qiu, P., Su, P., Li, Y., Lu, X., Chen, W., Ahmed, M. S., et al. (2025). Formation processes, accumulation patterns and risk mitigation strategies for harmful gases in tunnels within the complex geological structure area of Southwest China. *Bull. Eng. Geol. Environ.* 84, 282. doi:10.1007/s10064-025-04256-5
- Renchun, H., Xing, F., Fan, X., and Zou, Y. (2019). The establishment of high-resolution sequence stratigraphic framework and reef-bank reservoir prediction of Changxing-Feixianguan Formations in Yuanba area, Sichuan Basin. *Paleogeography* 21 (2), 369–378. doi:10.7605/gdxb.2019.02.021
- Richard, J. (2002). The san fernando tunnel explosion, California. *Eng. Geol.* 67 (1), 1–3. doi:10.1016/s0013-7952(02)00042-x
- Sabrekov, A. F., Terenteva, I. E., McDermid, G. J., Litt, Y. V., Prokushkin, A. S., Glagolev, M. V., et al. (2023). Methane in West Siberia terrestrial seeps: origin, transport, and metabolic pathways of production. *Glob. Change Biol.* 29 (18), 5334–5351. doi:10.1111/gcb.16863
- Shahriar, K., Rostami, J., and Khademi Hamidi, J. (2009). TBM Tunneling and analysis of high gas emission accident in Zagros long tunnel.
- Shijiazhuang Railway University (2016). *Research on construction technology of lijiaowan tunnel in bad geological section of songqingbo-bada railway*. Shijiazhuang Railway University, unpublished Master Thesis, 65.
- Sortino, F., Giammanco, S., Bonfanti, P., and Bottari, C. (2022). Stress-induced changes in hydrothermal gas discharges along active faults near Mt. Etna volcano (Sicily, Italy). *Tectonophysics* 836, 229388. doi:10.1016/j.tecto.2022.229388
- Su, P., Cao, J., Hongyi, S., Yuben, D., and Chen, H. (2020). Formation mechanism and migration mode of harmful gases in tunnels in non-coal strata in complex structural areas. *China Railw. Sci.* 41 (2), 91–98. doi:10.3969/j.issn.1001-4632.2020.02.11
- Su, P., Li, J., and Xu, Z. (2021). Occurrence regularity of shallow natural gas in non-coal strata and protection scheme of gas tunnel engineering. *Zhongguo Tiedao Kexue/China Railw. Sci.* (2), 88–97. doi:10.3969/j.issn.1001-4632.2021.02.10
- Sun, Z., Zhang, D., and Fang, Q. (2023). Technologies for large cross-section subsea tunnel construction using drilling and blasting method. *Tunn. Undergr. Space Technol.* 141, 105161. doi:10.1016/j.tust.2023.105161
- Talma, A. S., and Esterhuysen, C. (2015). Isotopic clues to the origin of methane emissions in the karoo. *South Afr. J. Geol.* 118 (1), 45–54. doi:10.2113/sgsjg.118.1.45
- Tan, K., Chen, J., Yao, J., Wu, Q., and Shi, J. (2022). Geochemical characteristics and genesis of natural gas in the upper triassic Xujiahe Formation in the Sichuan Basin. *Open Geosci.* 14 (1), 1061–1074. doi:10.1515/geo-2022-0405
- Wang, B., Chen, X., and Chen, J. (2020). Elastic characteristics and rock physics modeling of Jurassic tight sandstone in Sichuan Basin. *Geophys. J.* 63 (12), 4528–4539. doi:10.6038/cjg202000346
- Wang, E., Guo, T., Li, M., Xiong, L., Dong, X., Wang, T., et al. (2023). Reservoir characteristics and oil properties of a lacustrine shale system: early Jurassic black shale from the Sichuan Basin, SW China. *J. Asian Earth Sci.* 242, 105491. doi:10.1016/j.jseaes.2022.105491
- Xiao, H. (2019). Geochemical characteristics and geological significance of natural gas in Jurassic Shaximiao Formation in Sichuan Basin. *Petroleum J.* (5), 568–576. doi:10.7623/syxb201905006
- Yang, X. L. (2021). Geochemical characteristics and genesis of natural gas in the middle jurassic Shaximiao Formation, Sichuan Basin. *Geoscience Nat. Gas* (8), 1117–1126. doi:10.11764/j.issn.1672-1926.2021.03.017
- Yu, H., Yang, R., He, Z., Bao, H., Han, Y., Zhang, W., et al. (2023). Full-scale pore structure and fractal characteristics of continental organic-rich shale: a case study of the dongyuemiao member of jurassic Ziliujie Formation in the fuxing area, eastern Sichuan Basin. *Energy Fuels* 37 (14), 10426–10443. doi:10.1021/acs.energyfuels.3c01547
- Yuan, C., Zhang, G., and Song, Z. (2023). Study on the causes and characteristics of special gas disasters in complex tunnels in western sichuan. *J. Railw. Eng. Soc.* (8), 29–34. doi:10.3969/j.issn.1006-2106.2023.08.005
- Zhang, B., Pan, Ke, Wu, C., Wang, X., Tang, Y., Jizhen, Z., et al. (2022). Mechanism and model of natural gas composite accumulation in multi-stage sand group of Jurassic Shaximiao Formation in Jinjia gas field, Sichuan Basin. *Nat. Gas. Ind.* 42 (1), 51–61. doi:10.3787/j.issn.1000-0976.2022.01.005
- Zhang, B., Sun, H., and Luo, Q. (2023a). Geochemical characteristics and oil and gas sources of platform lagoon facies source rocks in Leikoupo Formation, central Sichuan. *Nat. Gas. Ind.* (6), 15–29. doi:10.3787/j.issn.1000-0976.2023.06.002
- Zhang, X., Deng, H., Xu, Z., Zhu, D., Duan, B., Wang, X., et al. (2023b). Accumulation and high-yield model of narrow channel tight sandstone gas controlled by “double-sources”: a case study of Middle Jurassic Shaximiao Formation of Jinjia gas field in the Sichuan Basin. *Nat. Gas. Ind.* 43 (10), 34–46.
- Zhou, G.-X., Wei, G.-Q., and Hu, G.-Y. (2019). Differences of continental hydrocarbon system between Longgang and Yuanba Gasfields in Sichuan Basin. *Nat. Gas. Geosci.* 30 (6), 809–818. doi:10.3787/j.issn.1000-0976.2019.10.004
- Zhou, Z., Li, Y., Lu, J., Wu, X., Zou, H., Hu, Z., et al. (2022). Origin and Genesis of the Permian Hydrocarbon in the Northeast of the Dongdaohaizi Depression, Junggar Basin, China. *ACS Omega* 7 (28), 24157–24173. doi:10.1021/acsomega.2c00725
- Zou, C., Chunchun, Xu, Wang, Z., Hu, S., Yang, G., Jun, Li, et al. (2011). Geological characteristics and forming conditions of the platform margin large reef-shoal gas province in the Sichuan Basin. *Petroleum Explor. Dev.* 38 (6), 641–651. doi:10.1016/s1876-3804(12)60001-9
- Zuo, S., Wang, Y., and Chen, D. (2023). Geochemical characteristics and genetic mechanism of natural gas in the superimposed oil and gas areas of the Western Sichuan Depression. *J. Northeast Petroleum Univ.* (1), 1–14. doi:10.3969/j.issn.2095-4107.2023.01.001